Available online at www.sciencedirect.com
SCIENCE DIRECT®
Physics of the Earth and Planetary Interiors 138 (2003) 39–54
PHYSICS OF THE EARTH AND PLANETARY INTERIORS
www.elsevier.com/locate/pepi

Secular variation in numerical geodynamo models with lateral variations of boundary heat flow

U.R. Christensen [a,b,*], P. Olson [c]

[a] *Institut für Geophysik, Georg-August Universität Göttingen, Herzberger Landstrasse 180, 37075 Göttingen, Germany*
[b] *Max-Planck-Institut für Aeronomie, Max-Planck-Strasse 2, 37191 Katlenburg-Lindau, Germany*
[c] *Department of Earth and Planetary Sciences, Johns Hopkins University, Baltimore, MD 21218, USA*

Received 2 October 2002; received in revised form 5 March 2003; accepted 5 March 2003

Abstract

We study magnetic field variations in numerical models of the geodynamo, with convection driven by nonuniform heat flow imposed at the outer boundary. We concentrate on cases with a boundary heat flow pattern derived from seismic anomalies in the lower mantle. At a Rayleigh number of about 100 times critical with respect to the onset of convection, the magnetic field is dominated by the axial dipole component and has a similar spectral distribution as Earth's historical magnetic field on the core-mantle boundary (CMB). The time scales of variation of the low-order Gauss coefficients in the model agree within a factor of two with observed values. We have determined the averaging time interval needed to delineate deviations from the axial dipole field caused by the boundary heterogeneity. An average over 2000 years (the archeomagnetic time scale) is barely sufficient to reveal the long-term nondipole field. The model shows reduced scatter in virtual geomagnetic pole positions (VGPs) in the central Pacific, consistent with the weak secular variation observed in the historical field. Longitudinal drift of magnetic field structures is episodic and differs between regions. Westward magnetic drift is most pronounced beneath the Atlantic in our model. Although frozen flux advection by the large-scale flow is generally insufficient to explain the magnetic drift rates, there are some exceptions. In particular, equatorial flux spot pairs produced by expulsion of toroidal magnetic field are rapidly advected westward in localized equatorial jets which we interpret as thermal winds.

Keywords: Geomagnetism; Geodynamo simulations; Paleomagnetic field; Core-mantle coupling

1. Introduction

The paleomagnetic and archeomagnetic records, as well as historical field measurements, suggest that persistent patterns of secular variation are present in the geomagnetic field over a range of time scales. The best known example is the apparent westward drift of nondipole magnetic field structures, particularly beneath the Atlantic. Another example is the low variability observed in the magnetic field beneath the mid-Pacific compared to other regions, the so-called Pacific dipole window. Persistent, regional differences such as these provide constraints on the mechanism of the geodynamo. Longitudinal differences in secular variation indicate a symmetry-breaking influence on the geodynamo, by thermal or electromagnetic core-mantle coupling, for example. A related issue

* Corresponding author. Tel.: +49-5556-979-542; fax: +49-5556-979-219.
E-mail addresses: christensen@linmpi.mpg.de (U.R. Christensen), olson@jhu.edu (P. Olson).

0031-9201/03/$ – see front matter © 2003 Elsevier Science B.V. All rights reserved.
doi:10.1016/S0031-9201(03)00064-5

is the time interval over which the geomagnetic field must be averaged to eliminate short-term transients and reveal the persistent nondipole field.

1.1. Secular variation of the Earth's field

The characteristic time scale of secular variation in the historic and archeomagnetic fields is defined at each spherical harmonic degree as (Hulot and LeMouël, 1994; Hongre et al., 1998; Carlut et al., 1999)

$$\tau_\ell = \sqrt{\frac{W_\ell}{\dot{W}_\ell}}, \tag{1}$$

where W_ℓ is the power in the magnetic field at degree ℓ, summed over harmonic order m (after Lowes, 1974), $\dot{W}_\ell$ the power of its time derivative, and τ is found to be in the range of 100–200 years for $\ell =$ 2–7, and decreases with increasing ℓ. The time constant of the equatorial dipole is slightly larger, about 400 years. Since the correlation between snapshots of the magnetic field vanishes when their time difference exceeds $\approx 3\tau$, an average over few thousand years is required to eliminate the transient secular variations, and reveal the persistent nondipole field (Carlut et al., 1999).

The amplitude of secular variation is usually characterized by the standard deviation of various elements of the magnetic field at a given site. Often the local field is represented by a virtual geomagnetic pole position (VGP), calculated from the local field direction by assuming a pure geocentric dipole field (Merrill et al., 1998). The scatter of VGPs, given by the angular standard deviation (ASD) at a site, is one measure of secular variation amplitude. VGP scatter typically depends on site latitude. In the recent paleomagnetic field, for example, the ASD increases by nearly a factor of two between the equator and the poles (Cox, 1970).

It is well established that secular variation in the historic field is weaker in the Pacific than elsewhere (Bloxham and Gubbins, 1985; Hulot et al., 2002). Because the non-dipole part of the surface field is presently low in the Pacific, this region has been referred to as the "Pacific non-dipole low" (McWilliams et al., 1982) or "Pacific dipole window" (McElhinny et al., 1996). Heterogeneity of the lower mantle, either in temperature (Doell and Cox, 1972; Bloxham and Gubbins, 1987) or in electrical conductivity (Runcorn, 1992), has been invoked to explain the Pacific dipole window. Both of these mechanisms are long-term, and imply the Pacific window should also be present in the paleomagnetic field. The evidence on this question is mixed, however. Low angular dispersion of VGPs have been derived for Hawaiian lavas from the Brunhes epoch (Doell and Cox, 1972; McWilliams et al., 1982), and support the interpretation of weak secular variation in the Pacific during that time. However, more recent analyses of paleomagnetic data generally find no significant differences in secular variations between the Pacific and other parts of the world (McElhinny et al., 1996; Herrero-Bervera and Valet, 2002). Constable and Johnson (1999) compare statistical models of secular variation with and without zonal variations and find that both are equally compatible with the existing global paleomagnetic lava data. From the analysis of a variety of data covering the last 3000 years, Constable et al. (2000) do not find reduced secular variation for the Pacific region. However, they suggest that regional differences in the standard deviations of magnetic elements do exist on this time scale.

Secular variation is often treated as a stochastic process, in which individual Gauss coefficients vary independently (Constable and Johnson, 1999). However, systematic secular variation has also been considered, in particular the apparent westward drift of the the geomagnetic field. Bullard et al. (1950) modeled the historical secular variation by a uniform westward drift of the non-dipole field at a rate of 0.2° per year. Yukutake and Tachinaka (1969) found a better fit by dividing the field into drifting and standing parts. These interpretations were based on secular variation at the Earth's surface. From the magnetic field at the core-mantle boundary (CMB), Bloxham et al. (1989) find that westward drift on the core surface is not global, but instead is restricted to the region between 120°E and 90°W, with typical rates around 0.2° per year. On other parts of the CMB, particularly in the Pacific hemisphere, Bloxham et al. (1989) find little or no westward drift. Even in the Atlantic hemisphere the drift is not uniform. Rapid westward drift is restricted to spots of concentrated magnetic flux located below Africa and the tropical Atlantic. These structures are assumed to result from expulsion of toroidal magnetic field across the CMB, analogous to sunspot formation

in the solar field (Bloxham, 1986; Christensen et al., 1998).

1.2. Secular variation in dynamo models

Numerical dynamos exhibit secular variation comparable to the observed geomagnetic secular variation. For example, Kuang and Bloxham (1998) obtained a rate of secular variation approximately half of the observed rate in a dynamo model with homogeneous boundary conditions. Hemispherical differences in secular variation, with quiet and active hemispheres, persist for about 500 years in their model, and their magnetic field has an apparent westward drift of about 0.2° per year. Bloxham (2000) compared models with homogeneous boundaries to models with a heterogeneous outer thermal boundary condition derived from the seismic structure of the lower mantle. Bloxham (2000) finds that the standard deviation of inclination is too small in models with homogeneous boundary conditions, but comparable to the measured variance in models with heterogeneous boundary heat flow. In addition, he finds that that heterogeneous boundary heat flow produces smaller inclination anomalies, i.e. deviations from inclinations predicted for an axial dipole field, in the Pacific hemisphere than elsewhere.

Kono et al. (2000) find both eastward and westward drift of magnetic structures in the dynamo model of Sakuraba and Kono (1999). They obtain a higher statistical variance for the g_2^1 and h_2^1 Gauss coefficients than for the other quadrupole terms, which has been shown to explain the observed latitudinal variation of the VGP scatter (Quidelleur and Courtillot, 1996). Kono and Roberts (2002) calculate this scatter for dynamo models by Sakuraba and Kono (1999) and Glatzmaier et al. (1999). For the Glatzmaier et al. (1999) model they find only a very weak latitude dependence, whereas in the Sakuraba and Kono (1999) model the increase of VGP dispersion with latitude is even stronger than in the paleomagnetic record. Kono and Roberts (2002) also analyze the model of Glatzmaier et al. with respect to systematic migration of magnetic structures. They find dominant westward drift, even though the zonal flow in that dynamo is mainly eastward, an effect they attribute to wave propagation in the field. Wave propagation in the magnetic field was also invoked by Olson et al. (1999) to explain the apparent drift of field structures over a short time interval in their dynamo model.

In a previous paper (Olson and Christensen, 2002) we used numerical dynamo models with heterogeneous heat flow conditions on the outer boundary to determine the pattern of the time average magnetic field. We found that a zonal variation of the heat flow influences the axial quadrupole and octupole contributions to the long-term magnetic field, while non-zonal differences in the heat flow give rise to the formation of "flux lobes" at high latitudes in the time average magnetic field. Here we use a similar model to assess the influence of lateral variations in thermal forcing on the temporal fluctuations of the magnetic field.

2. The dynamo model

The basic concept of our dynamo model has been described in Olson et al. (1999) and Christensen et al. (1999). We simulate three-dimensional, time-dependent thermal convection and magnetic field generation in an rotating spherical shell filled with an electrically conducting Boussinessq fluid. The ratio of inner and outer shell radius is $r_\mathrm{i}/r_\mathrm{o} = 0.35$. We solve the Navier–Stokes equation with full inertia, Coriolis and Lorentz forces, and uniform Newtonian viscosity, coupled to the heat transport equation and the magnetic induction equation. Both spherical boundaries are rigid, impermeable, and electrically insulating. Heat flow is prescribed on the outer boundary, and on the inner boundary we prescribe a fixed uniform temperature. We employ a spectral transform method for solving the equations, using a radial grid with N_r grid levels and expanding all variables in spherical harmonics up to degree and order ℓ_max.

As described in Olson and Christensen (2002), we impose on the outer boundary a heat flow q that is composed of the mean part q_o plus a spatially variable part $q'(\theta, \phi)$. In Olson and Christensen (2002) we compared models with different patterns and amplitudes of q'. Here we concentrate on the so-called "tomographic" case, where the pattern of q' is derived from the first four spherical harmonic degrees in the Masters et al. (1996) model of seismic shear wave heterogeneity at the base of the mantle (Fig. 1). We fixed the amplitude of q' such that that the peak-to-peak difference of heat flow in the dominant term harmonic

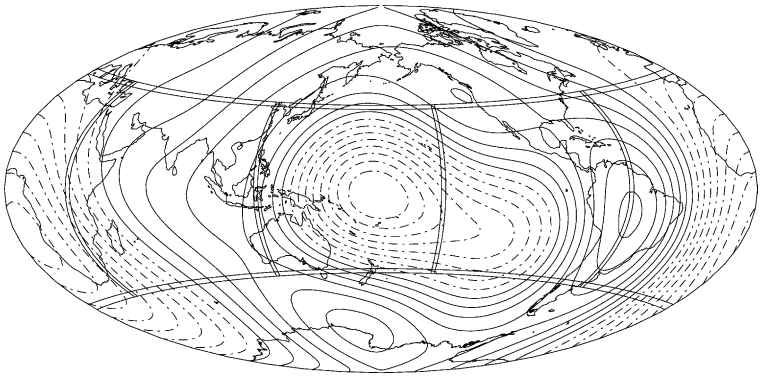

Fig. 1. Deviation of imposed heat flow from the mean value q_o. Contour step is $q_o/10$; broken lines indicate lower than average heat flow. Four quadrants used for the analysis of westward drift are delineated.

degree and order two equals q_o. The rms amplitude of the heat flow variation is 27% of the mean, and the maximum and minimum values of q are around 1.6 and 0.1 times q_o, respectively.

The equations are scaled using the shell thickness D as length scale and the magnetic diffusion time D^2/η, with η the magnetic diffusivity, as time scale. The magnetic field $\boldsymbol{B}$ is scaled by $\sqrt{\rho\Omega/\sigma}$, where σ is the electrical conductivity, Ω the rotation frequency, and ρ is the density. With this scaling, dimensionless control parameters are the Rayleigh number

$$Ra = \frac{\alpha g_o q_o D^4}{k\kappa\nu}, \tag{2}$$

the Ekman number

$$E = \frac{\nu}{\Omega D^2}, \tag{3}$$

the Prandtl number

$$Pr = \frac{\nu}{\kappa}, \tag{4}$$

and the magnetic Prandtl number

$$Pr_m = \frac{\nu}{\eta}. \tag{5}$$

Here α is the thermal expansivity, g_o gravity on the outer boundary, k thermal conductivity, κ thermal diffusivity, and ν is viscosity.

We have calculated four different dynamo cases, although we concentrate our analysis on one, the reference tomographic model. This is the case referred to in the following discussion, unless we indicate otherwise explicitly. For the reference tomographic case we adopt the following parameter values: $Ra = 2.84 \times 10^7$, $E = 10^{-4}$, $Pr = 1$, $Pr_m = 2$. The model is similar to the tomographic model in Olson and Christensen (2002), except that the Ekman number is now lower, i.e. slightly less remote from Earth values. To maintain a similar degree of supercriticality at a lower E, the Rayleigh number has been increased. The critical value of the Rayleigh number, $Ra_c = 243{,}800$, applies to the onset of convection for a homogeneous heat flow condition without magnetic field. Note that the Rayleigh number is defined here based on the boundary heat flow; its value based on the mean temperature drop across the shell is lower and corresponds to 22× instead of 117× supercritical. The reference model was started from a dynamo with similar parameters but fixed temperature boundary conditions. The simulation was run for about 0.25 magnetic diffusion times with the new parameters. After this time the system has adjusted to the new conditions, as suggested, for example, by the stabilisation of non-zero time-averaged values for some of the low-order non-zonal Gauss coefficients (see below). The run was then continued for another 2.5 diffusion times, and the results from this period were analyzed as described below. In addition we examined two cases with lower and higher Rayleigh number, respectively, all other parameters being equal. We have also run a case with homogeneous heat flow on the outer boundary at the parameter values of the reference model. These additional models were run for about 0.5 magnetic diffusion time beyond the initial transient adjustment.

This time proved sufficient to estimate some statistical properties of the secular variation. Finally, we note that all of our models have reversed dipole polarity (relative to the present geomagnetic field), a consequence of our initial conditions. The dipole polarity has no effect on our analysis or our interpretations.

3. Results

Summary properties of the four models are given in Table 1. The magnetic Reynolds number $Rm = vD/\eta$ refers to the dimensionless average (rms) fluid velocity. Also listed is the dimensionless average (rms) magnetic field strength (the square root of the Elsasser number) for the whole fluid $\bar{B}$ and on the outer boundary $\bar{B}_{\rm cmb}$, and the axial dipole field on the outer boundary $B_{\rm dip}$, respectively.

The reference model generates a magnetic field dominated by the axial dipole, which contributes approximately 50% to the magnetic field strength at the outer shell boundary. The dipole intensity, when scaled with a core electrical conductivity of $\sigma = 6 \times 10^5$ S/m (Secco and Schloessin, 1989), is about twice as strong as the geomagnetic dipole on the CMB. The power spectrum of the magnetic field on the outer boundary has similarities to the spectrum of Earth's field at the CMB: in addition to dipole dominance and a comparatively weak quadrupole, the spectrum is nearly white up to harmonic degree 12 (Fig. 2). The presentation is truncated at degree 12, because higher harmonics of the Earth's core field are shielded by crustal magnetisation. The low-order harmonics other than the dipole are slightly enhanced in the model with heterogeneous heat flow compared to the homogeneous case. Global spectra of kinetic and magnetic energy drop by at least two orders of magnitude up to degree $\ell_{\rm max}$, indicating sufficient resolution. We do not observe reversals and excursions of the magnetic dipole in the reference model, and the tilt of the dipole axis never exceeds 20°.

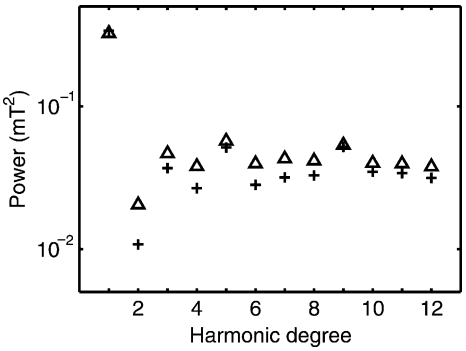

Fig. 2. Time average magnetic power spectra at the outer model boundary for the tomographic reference model (triangles) and the homogeneous case (crosses).

The case with low Rayleigh number and with homogeneous heat flow show a similar strength and geometry of the magnetic field. However, when the Rayleigh number is increased the dynamo regime changes, as was found by Kutzner and Christensen (2002) for various thermal boundary conditions. In the high Rayleigh number case the dipole contribution to the magnetic field becomes relatively weak and its direction fluctuates strongly. Because of this behavior, the high Rayleigh number case is ill-suited for comparison with geomagnetic secular variation during periods of stable polarity.

3.1. Time scale of secular variation

We calculated the time scale of secular variation as a function of harmonic degree for our models from Eq. (1), using the time average power of the magnetic field W_ℓ at harmonic degree ℓ and the time average power of its time derivative $\dot{W}_\ell$. Results are shown in Fig. 3. Only the equatorial dipole has been used in

Table 1
Summary of model runs

Case	Ra	Ra/Ra_c	Heat flow	N_r	$\ell_{\rm max}$	Rm	$\bar{B}$	$\bar{B}_{\rm cmb}$	$B_{\rm dip}$
Reference	2.84×10^7	117	Tomographic	41	85	320	3.5	1.20	0.55
Homogeneous	2.84×10^7	117	Uniform	41	85	325	3.2	1.13	0.55
Low Ra	1.44×10^7	59	Tomographic	41	64	218	3.5	1.28	0.60
High Ra	7.18×10^7	295	Tomographic	49	106	660	2.7	0.67	0.09

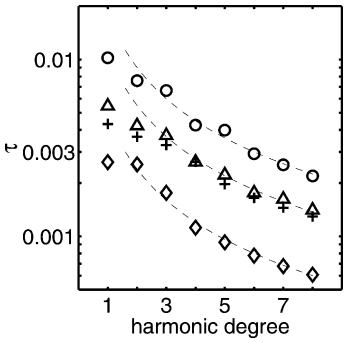

Fig. 3. Time scale τ of secular variation (in magnetic diffusion times) vs. spherical harmonic degree. Triangles denote the tomographic reference model, crosses the homogeneous case, circles the case of low Rayleigh number and diamonds the high Rayleigh number tomographic cases, respectively. Broken lines show fits to $\tau_\ell \propto \ell^{-1}$ for $\ell > 2$.

calculating τ_1; including the axial dipole would increase τ_1 by almost an order of magnitude.

Fig. 3 shows that the time scale of secular variation becomes shorter with increasing harmonic degree, as in the historic and archeomagnetic fields. Beyond harmonic degree two, τ_ℓ decreases approximately as $\tau_o \ell^{-1}$, with $\tau_o = 0.018$ in the low Rayleigh number case, 0.011 in the reference model, and 0.0048 in the high Rayleigh number case, respectively. The dipole term shows a somewhat faster variation (smaller τ_1 than our fit predicts). For degrees >3, the time scales in the homogeneous boundary case are the same as the reference case, but secular variation of the low-order terms is slightly weaker in the inhomogeneous case. This indicates that the boundary heat flow pattern generates a stable large-scale structure in the magnetic field. Assuming that secular variation is mainly due to the advection of magnetic field by the larger-scale flow, the time scales should vary as the inverse of the magnetic Reynolds number Rm^{-1}. Comparing our results at the three different Rayleigh numbers suggests a slightly stronger dependence on Rm than this.

With $\sigma = 6 \times 10^5$ S/m, one magnetic diffusion time corresponds to ~122,000 years in the core. Using this factor to scale time, τ_ℓ in the reference model are 660 years for the equatorial dipole, 500 years for the quadrupole and about 200 years at $\ell = 8$. These are larger than historic field values by roughly a factor of two. This discrepancy is expected, since the magnetic Reynolds number $Rm = 320$ in our reference model is about a factor of two smaller than in the core, when the core value is based on our assumed conductivity and a velocity equivalent to 0.2° per year of drift. In the high Rayleigh number case, Rm is more Earth-like, and the time scales τ are in better agreement with the observed secular variation. However, this model has a weak and highly variable dipole field, which is not particularly Earth-like. Kutzner and Christensen (2002) have shown that transition to weak dipole fields generally occurs at high Rayleigh number, and the transition Rayleigh number increases with decreasing Ekman number. Therefore, we anticipate that stable dipolar dynamos with Earth-like values of Rm will be found at a lower Ekman number than we use here. Unfortunately, a dynamo calculation for these parameters covering several magnetic diffusion times is now prohibitively time-consuming.

In order to rationalize the factor two discrepancy in the magnetic Reynolds number between our reference model and the Earth, we can use the advective time scale for converting dimensionless time into Earth time, rather than the diffusive time scale. Based on the advection time scale, one nondimensional time unit is equivalent to about 60,000 years. We now adopt this factor for time scaling in the reference case.

We note, however, that potentially important processes at short time scales cannot be properly scaled to the Earth because of the difference in control parameters, such as a large Ekman number in the model. For example, inertial modes in the Earth's core have a time scale of a day and cannot lead to observable variations of the internal magnetic field. In our model, when scaled to real time using the magnetic diffusion time scale, one "day" (rotation period) is equivalent to ≈200 years. Therefore some of the secular variation seen in our model might be associated with inertial waves. Torsional oscillations in the Earth's core may contribute to the geomagnetic variation (e.g. Zatman and Bloxham, 1997). Here the time scales are roughly correct in our models, but the enhanced viscosity implied by the high Ekman number may damp them to a disproportional degree.

Fig. 4 shows the time average radial magnetic field at the outer boundary of the model, restricted to spherical harmonic degrees up to 12, for different lengths of the averaging interval. The long-term average in Fig. 4d is very similar to the result obtained in Olson and Christensen (2002) for the same

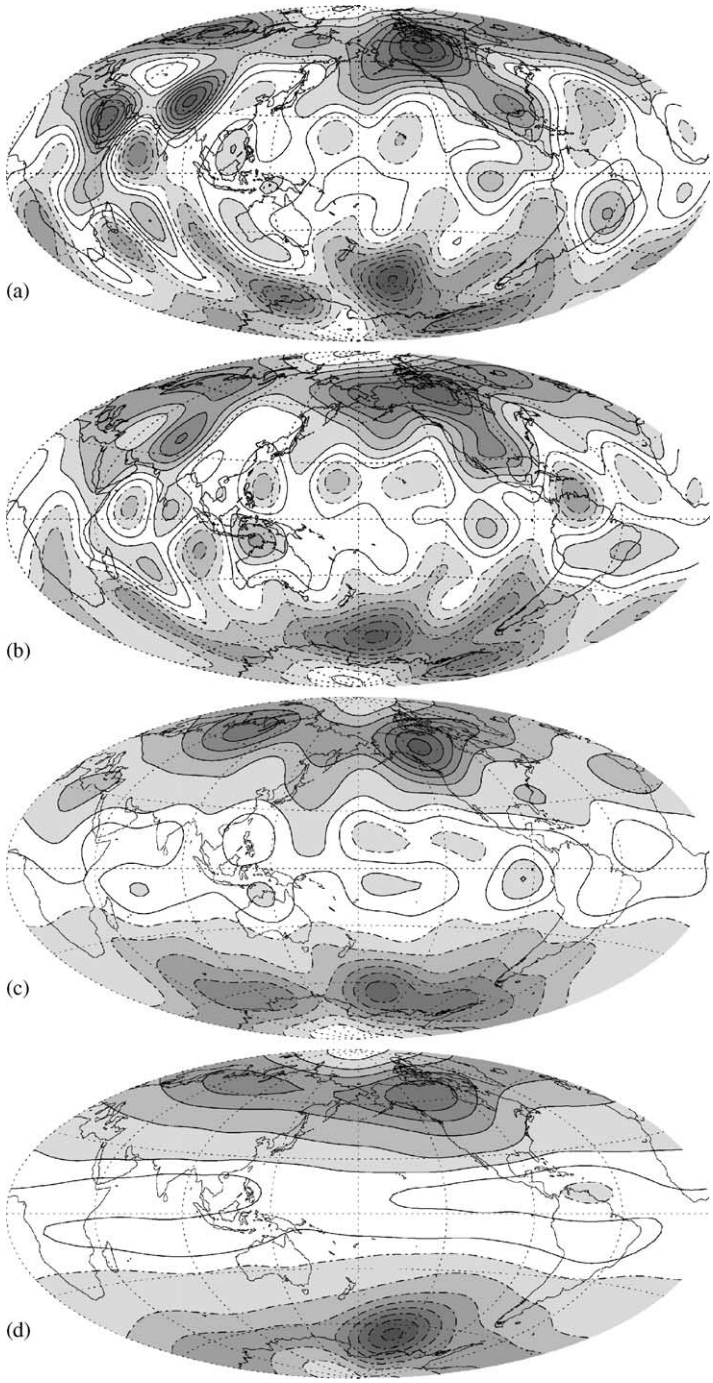

Fig. 4. Radial magnetic field at the core-mantle boundary truncated at $\ell = 12$ from the reference tomographic dynamo model. Broken contours indicate negative values, solid contours indicate zero and positive values. The contour interval is 0.22 and greyscale highlights large absolute values: (a) snapshot, time averages over; (b) $\Delta t = 0.004$ (240 years); (c) $\Delta t = 0.034$ (2000 years); (d) $\Delta t = 2.5$ (150,000 years).

pattern of heat flow heterogeneity but different values of the Ekman number and Rayleigh number. In particular, two flux lobes are evident in the northern hemisphere, one beneath North America and a weaker one beneath Russia. There is a single strong flux patch in the southern hemisphere. The flux patches are not stationary. An animation showing the variation of the magnetic field with time reveals that these flux concentrations change shape and move around within a confined region, so that their positions in the long-term average field reflect the average of their instantaneous locations. Fig. 4a shows an instantaneous snapshot of the magnetic field. Fig. 4b and c show successively longer averaging intervals which we call the "historic window" (240 years) and the "archeomagnetic window" (2000 years), respectively. Smaller scales in the field are progressively suppressed as the averaging interval is lengthened. The three flux concentrations in the long-term field are recognizable in the snapshot and also in the historic window. In the archeomagnetic window, much of the transient small-scale structure has been averaged out, so the persistent high-latitude flux concentrations stand out clearly. However, an additional southern hemisphere flux patch is visible in this window, which is not evident in the long-term field.

A more rigorous test of how long the magnetic field must be averaged to reveal a persistent nondipole component is to calculate the average values of low-order Gauss coefficients over different time windows Δt. We chose $\Delta t = 0.0006$ (360 years) for the historical window, 0.03 (1800 years) for the archeomagnetic window and 0.3 (18,000 years) for a longer-term average. The time series of Gauss coefficients was saved in steps of 20 years and subdivided into 400, 80 and 8 intervals, respectively. The mean of the Gauss coefficients has been calculated in each time interval separately, which gives us a distribution of averages for each g_ℓ^m. From this distribution the standard deviation from the global mean was determined. For the historical window (Fig. 5a) the only coefficient which is nonzero at the 2σ significance level (apart from g_1^0) is the axial octupole g_3^0. The axial octupole is the largest persistent deviation from a pure axial dipole in our models with and without heat flow heterogeneity (Olson and Christensen, 2002). This contrasts with the geodynamo, where several analyses found the axial quadrupole to be the most significant

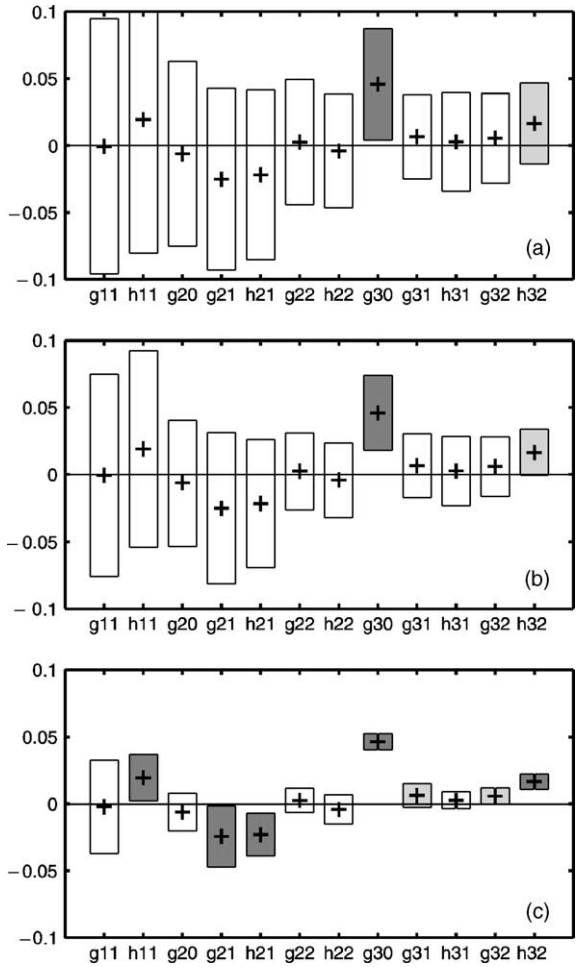

Fig. 5. Crosses show the long-term mean of Gauss coefficients, normalized the by average g_1^0. Bars indicate twice the standard deviation (2σ) of averages obtained for various time intervals: (a) $\Delta t = 0.006$ (360 years); (b) $\Delta t = 0.03$ (1800 years); (c) $\Delta t = 0.3$ (18,000 years). Dark shading indicates significance of non-zero means at the 2σ-level and light shading significance at the 1σ-level.

nondipole term (Merrill et al., 1998; Johnson and Constable, 1995). Aside from g_3^0, no other coefficient has a significant non-zero mean in the historical window. The situation is basically the same for the archeomagnetic window, although the coefficient h_3^2 is marginally significant at the 2σ-level. But when the window is lengthened to 18,000 years, significant non-zero values are found for several Gauss coefficients, including h_3^2, g_2^1 and h_2^1. These terms are the main contributors to the high-latitude flux lobes.

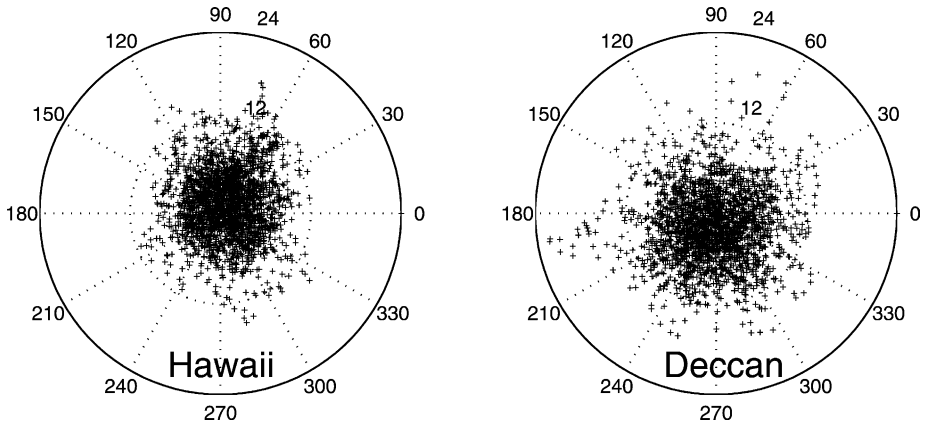

Fig. 6. Scatter of VGPs from the reference tomographic model at 19°N, 165°W (Hawaii) and at 18°N, 85°E (Deccan, India). The outer circle corresponds to 24° distance from the geographic pole.

3.2. Secular variation anomalies

Our model exhibits regional differences in the amplitude of secular variation that might be observable. To facilitate comparison with paleomagnetic or archeomagnetic data, we continue a representation of the model field to degree and order eight upwards to the Earth's surface, and calculate inclination and declination of the magnetic field vector at a large number of sites over the Earth surface. From these we determine the virtual geomagnetic pole position at each site. We break the model run into steps of approximately 60 years, which provides ≈2500 VGP positions at each site. In Fig. 6 we show the scatter of VGP positions for two sites in the equatorial region, corresponding to Hawaii and India. Although the differences are not large, the scatter is slightly bigger at India than at Hawaii.

We also calculate the angular standard deviation of the virtual geomagnetic pole positions at each site. The global distribution of ASD is shown in Fig. 7a. The ASD amplitude varies between 5.5 and 9°, which is about one-half of the range in the paelomagnetic record (Merrill et al., 1998). The primary variation in ASD is zonal, increasing with latitude, as seen in the paleomagnetic record. In addition, we find a weak non-zonal variation of about 1°. It is perhaps significant that in our model the lowest secular variation is found in the mid-Pacific, since the secular variation is low in this region in the historical geomagnetic field. Note that the longitude of maximum VGP scatter coincides with the strongest two flux lobes, a consequence of the time variability of these features.

Constable and Johnson (1999) argued that the dispersion of inclinations is more sensitive than VGP dispersion in revealing longitudinal variations in secular variation. We show the dispersion of inclinations from our model in Fig. 7b. Once again, zonal variations dominate, with a standard deviation of about 8° at the equator and 3° near the poles. The variation with longitude is slightly larger than in case of the VGP scatter. For comparison, in our dynamo model with uniform boundary heat flow, the standard deviation of inclinations is somewhat smaller than in Fig. 7b, and varies between 6° at low latitude and 2.5° at the poles. Higher inclination anomalies in dynamo models with inhomogeneous boundary conditions were also found by Bloxham (2000).

In the reference tomographic model, the regions with weak secular variation coincide with the regions of low heat flow (and elevated lower mantle temperatures) in the Pacific and the Atlantic (Fig. 1). Convection is more sluggish below the core-mantle boundary in these regions, compared to high heat flow regions, and this leads to reduced secular variation in the local magnetic field.

Bloxham (2000) used the same pattern of heat flow heterogeneity in his dynamo model as we do. He found that the time average inclination anomaly, that is the difference between inclinations calculated from

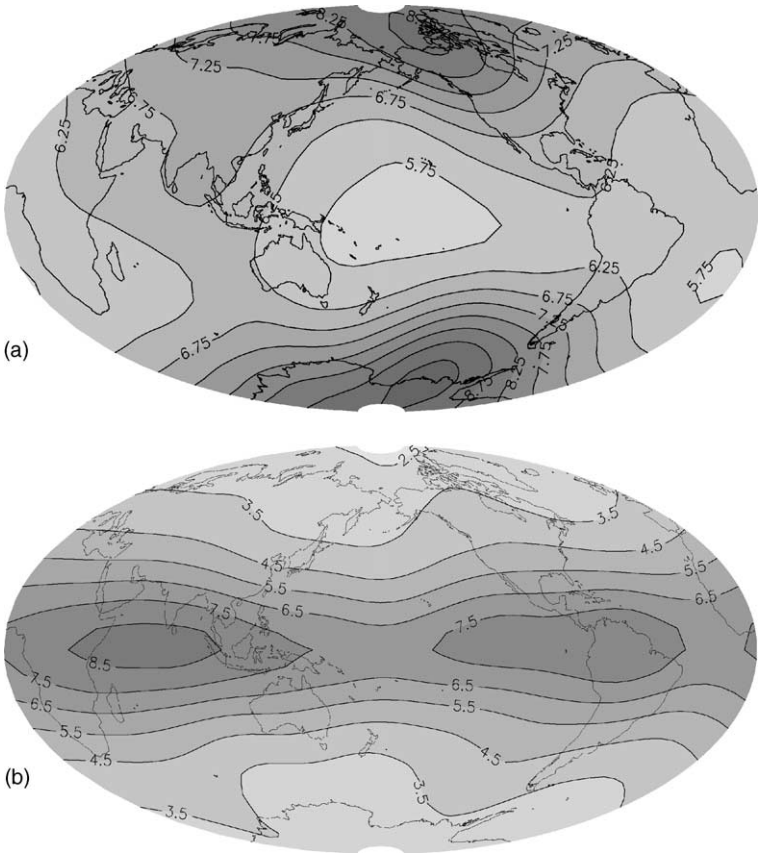

Fig. 7. (a) Global distribution of angular standard deviation (ASD) of virtual geomagnetic pole positions (VGPs) in degrees calculated from the reference model for points at the Earth's surface. (b) Standard deviation of inclinations.

the model and those of an axial dipole field, was lower in the Pacific than elsewhere. For our model we find roughly a similar pattern of inclination anomalies (Fig. 8). However, it is somewhat misleading to argue for a "dipole window" on the basis of small inclination anomalies in the Pacific. For example, the small values in the south Pacific seem to be due to a cancellation of the generally positive inclination anomaly in the southern hemisphere, resulting from the octupole component of the time average field, and the very pronounced (non-dipolar) contribution from the concentrated flux lobe in this region (cf. Fig. 4d). If instead of the octupole the axial quadrupole determines the zonal part of the inclination anomaly, as it does in the case of Earth's mean paleofield, the flux lobe would cause an enhanced inclination anomaly in the south Pacific.

3.3. Westward drift

An animation of the reference case shows that westward drift of magnetic field structures at the core-mantle boundary is more common than eastward drift, but both are intermittent and tend to occur at low latitudes and in restricted longitude bands. Rapid westward drift is best seen in the transient motion of pairs of equatorial flux spots. We quantify the drift rate of magnetic field structures within $\pm 40^\circ$ of the equator by dividing the region into four quadrants, from -60 to $+30^\circ$E (Atlantic), 30 to 120°E (Indian), 120 to 210°E (west Pacific), and from 210 to 300°E (east Pacific), respectively (Fig. 1). In each quadrant we use pairs of snapshots of the radial magnetic field on the outer boundary, separated in time by Δt. We calculate the cross correlation of $B_r(\theta, \phi - \Delta\phi/2, t)$

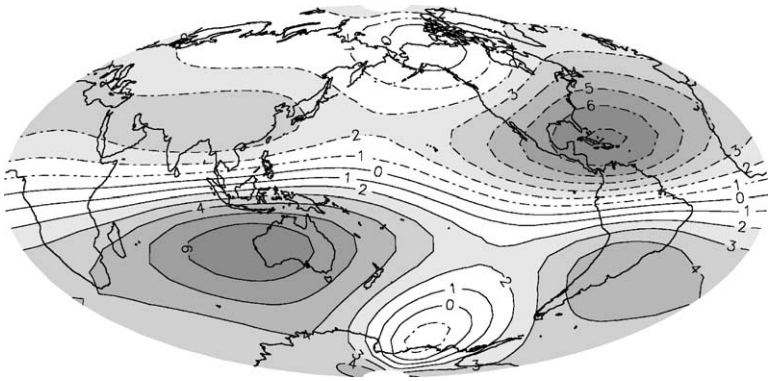

Fig. 8. Difference between inclinations of the time average dynamo field and an axial dipole field at the Earth's surface.

with $B_r(\theta, \phi + \Delta\phi/2, t + \Delta t)$, to find the optimum phase shift $\Delta\phi$ and the drift rate $\Delta\phi/\Delta t$ for that quadrant. We use $\Delta t = 0.001$, equivalent to 60 years, and varied $\Delta\phi$ in steps of 1.41° (the numerical grid interval). The maximum correlation coefficient is about 0.88 in each quadrant. Fig. 9 shows histograms of the drift rates found for each quadrant.

The magnetic drift is clearly not uniform in space or time in our model. In the Atlantic quadrant, only westward drift is found, with rates between 0 and −0.2° per year. The Indian and west Pacific quadrants show mainly westward drift, but with occasional episodes of eastward drift. In contrast, drift in the east Pacific quadrant is more frequently to the east. The mean drift

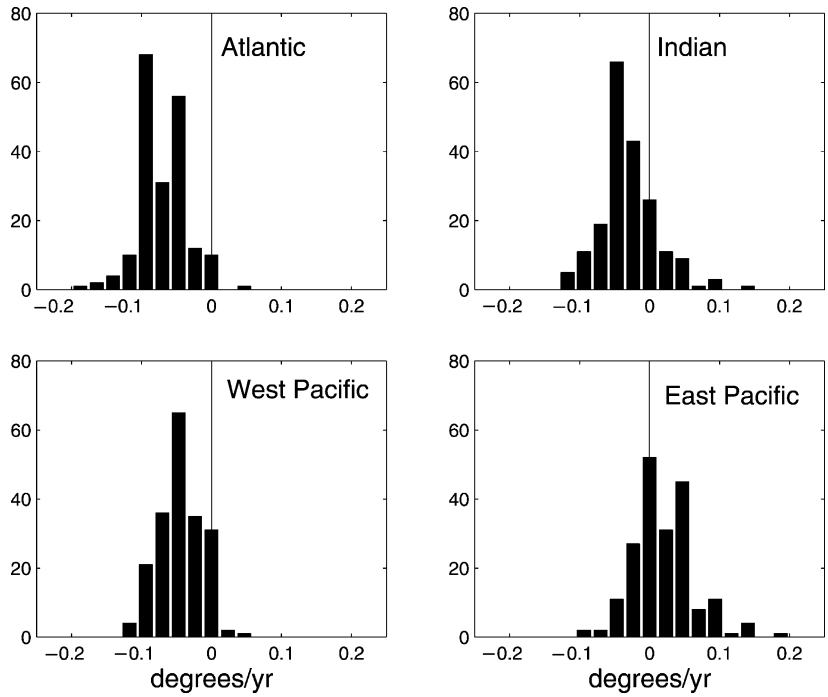

Fig. 9. Distribution of drift rates of low latitude magnetic field structures on the outer boundary of the reference tomographic dynamo model in four longitude sectors.

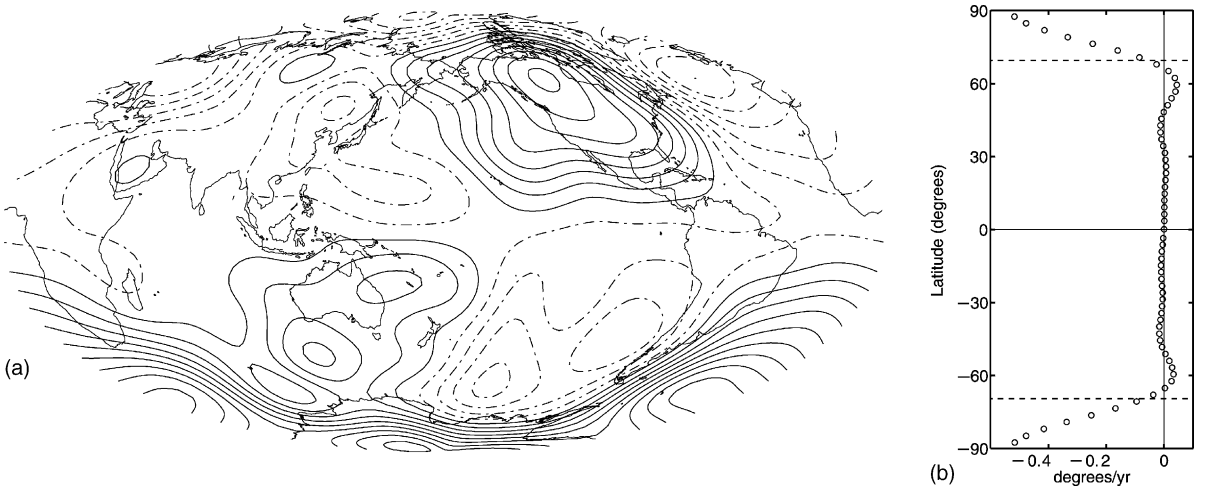

Fig. 10. (a) Streamlines of time average toroidal flow at 0.965 of the outer radius. Contour interval is six non-dimensional units and the circulation is anticlockwise along full lines and clockwise for broken lines. (b) Angular velocity for the zonal part of the time average flow vs. latitude.

rates are −0.07, −0.03, −0.045 and +0.02° per year, for the Atlantic, Indian, west Pacific and east Pacific, respectively. These values are smaller than the rates estimated for westward drift of the historical geomagnetic field (about −0.2° per year), although the most frequent drift rate in the Atlantic in our model is about one-half of the geomagnetic rate.

The mean drift rates can be compared with the mean flow near the surface of the model. Fig. 10a shows the time average toroidal flow near the outer surface (below the Ekman boundary layer) during the same time interval we analyzed the magnetic drift. We neglect the poloidal contribution here, since its time average is much smaller except at latitudes above 60°. We also show the zonal angular velocity, the azimuthally averaged net rotation rate of the fluid relative to the outer boundary (Fig. 10b). The zonal angular velocity is large only near the poles, where it is associated with a thermal wind flow inside the inner core tangent cylinder. Outside the tangent cylinder the time average zonal angular velocity is quite small. We note that this velocity pattern is very similar to the pattern recently derived from an inversion of satellite-derived secular variation data (Hulot et al., 2002), although the peak amplitude is lower in our model. The mean azimuthal flow between −40 and +40° latitude is −0.016° per year in the Atlantic, −0.005° per year in the Indian, −0.001° per year in the west Pacific and +0.013° per year in the east Pacific, respectively. The flow direction agrees with direction of magnetic drift in each quadrant. However, the fluid angular velocity is too small to explain the magnetic drift by passive, frozen flux advection, except in the east Pacific. This result supports the conjecture that the magnetic drift includes both frozen flux advection and a wave propagation effect. Although the dominant contribution to the imposed heat flow anomaly is in harmonic degree and order two, the mean magnetic drift or the mean advection rate in the four quadrants shows little hemispherical symmetry. We note that, for example, the African low heat flow anomaly extends much further polewards than the corresponding Pacific low and that the heat flow maximum under South America has higher amplitude than the one in the Indian ocean (Fig. 1). Such differences must be the cause why drift in the Atlantic is more pronounced than in the (west) Pacific.

Closer inspection of one particular episode of rapid drift in the Atlantic quadrant suggests a more direct relation between fluid motion and magnetic drift. Fig. 11a and b shows the westward drift of equatorial magnetic flux spots on the CMB during a short interval, 0.0008 magnetic diffusion time. The strong flux concentration marked by a white plus sign drifts by approximately 8–10° westward, while other spots

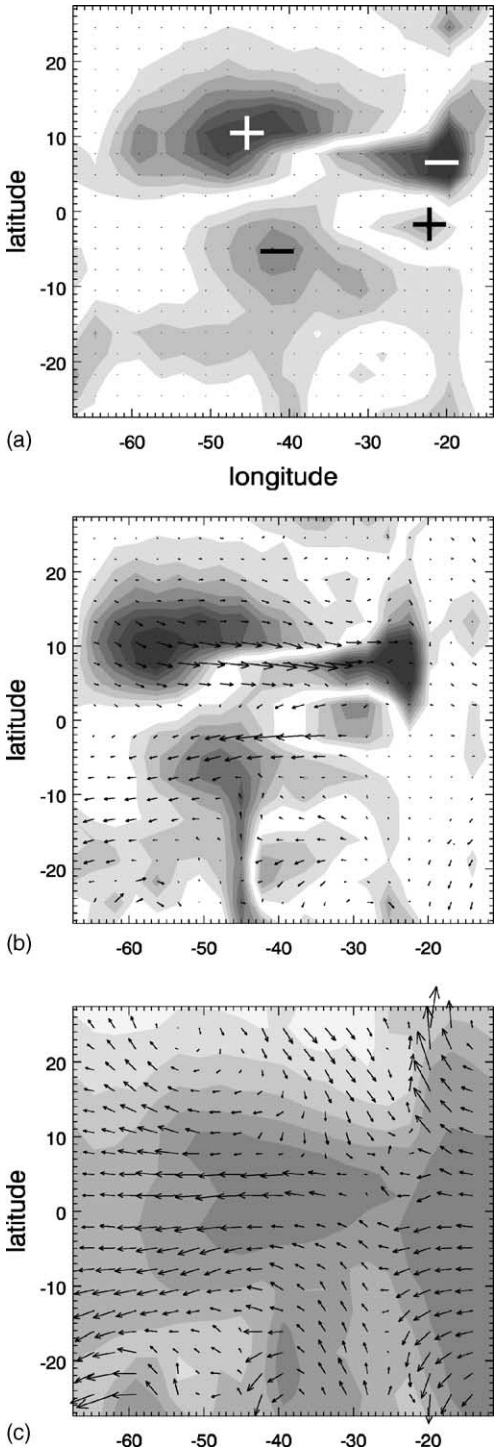

migrate less rapidly but in the same direction. The rapidly migrating spot is transported by a strong westward equatorial jet (Fig. 11c). The jet velocity at the magnetic spot, ≈300, is close to the magnetic drift rate there. At least in this one instance, and possibly in other rapid drift events near the equator, the drift seems to be dominantly by frozen flux advection. This conclusion can be reconciled with the fact that the average zonal flow is very weak, since strongly westward flow near the core-mantle boundary is localized in a few equatorial jets and the particularly strong flux spots tend to form in these jets. In this situation, rapid westward drift of a few such spots creates the impression of an overall westward drift at the Earth's surface.

The intense low-latitude flux spots are connected to very strong azimuthal magnetic flux tubes in the fluid beneath the outer boundary (Fig. 1b). These flux tube segments occur as nearly antiparallel pairs, one on either side of the equator. In the polarity of this calculation (reversed compared to the present-day geomagnetic field) the flux in the tube north of the equator points eastward, and the flux in the southern tube points westward. The tubes contribute to the axisymmetric toroidal magnetic field; however they are not axisymmetric themselves, but instead are bent and twisted by the convection. The fields within the tubes are quite intense. For example, the peak value of the azimuthal field in the tubes (≈15 in dimensionless units) is much larger than the maximum radial field on the outer boundary (≈1.8 in the same units).

The flux tubes are transported radially outward from the interior of the shell by broad-scale upwellings in the time-averaged circulation. These broad-scale upwellings are responsible for the equatorial flux spots, and they are indirectly responsible for their westward drift. The equatorial flux spots form by expulsion of bent portions of the flux tubes. As the flux tubes are brought close to the outer boundary by broad-scale

Fig. 11. Closeup views of B_r on the outer boundary, filtered to $\ell \leq 24$, 0.0008 time units apart (a, b). Greyscale shows intensity in steps of 0.25. In (a) the sign of flux is indicated for various spots. In (b) the horizontal component of the magnetic field at $r/r_o = 0.965$ is also shown; the longest arrow corresponds to $B \approx 15$. (c) Temperature on the outer boundary, contours step 0.033, darker shading is hotter. Arrows indicate horizontal flow at $r/r_o = 0.965$, longest arrow corresponds to $v \approx 800$.

upwellings, smaller-scale convective motions distort the tubes, producing a spatially varying radial component to the field. This radial field diffuses across the outer boundary and the field lines reconnect outside of the fluid, creating the flux-connected pairs of radial field spots shown in Fig. 11.

Fig. 11c shows that the fluid near the equator and beneath the flux spots is relatively hot. High equatorial temperatures are consistent with upwelling motion there, and also provide the driving force for the westward equatorial jet. The dimensionless thermal wind balance for azimuthal flow near the equator is, in terms of our scaling

$$2\frac{\partial u_\phi}{\partial z} \simeq -ERa\frac{\partial T}{\partial z} \tag{6}$$

where $\partial u_\phi/\partial z$ is the variation in the azimuthal velocity in the direction of the rotation axis and $\partial T/\partial z$ is the variation in temperature along the same direction. The jet velocity at the equator is therefore given by

$$u_{\mathrm{eq}} \simeq -\tfrac{1}{2}EraT' \tag{7}$$

where T' is the dimensionless equatorial temperature anomaly. For the equatorial temperature anomaly in Fig. 11c of about 0.14, (7) gives $u_{\mathrm{eq}} \simeq -200$, comparable to the maximum jet velocity of -300.

4. Conclusions

Secular variation in our reference tomographic model is characterized by roughly comparable time scales and amplitudes as the geomagnetic secular variation. Specifically, the model time scales are twice those of the historical and the archeomagnetic fields. We find that the model time scales decrease with increasing magnetic Reynolds number *Rm*. We therefore conclude that *Rm* in our model is less than in the core, by roughly a factor of two. The discrepancy can be corrected by interpreting model time using the advective time scale, rather than the diffusive time scale. The amplitude of secular variation, measured by the angular standard deviation of virtual geomagnetic pole positions, increases with latitude from about 6° at low latitude to 9° at high latitudes in our model. The same latitudinal dependence is found in the paleomagnetic record, but with a variation between 13 and 22° (Kono and Roberts, 2002; Quidelleur et al., 1994). However, we note that the standard deviations in inclinations found for our model, about 8° at the equator and 3° at the poles, is very similar to what Constable et al. (2000) found for the archeomagnetic field. Our model is probably more representative of the stable dipolar configuration of the geomagnetic field during the last 3000 years than of the long-term paleomagnetic field, where episodes of less stable field directions may contribute strongly to the scatter of VGP positions. Although there are differences in secular variation between our tomographic model and the geodynamo, there are many points of similarity. In this respect it is also encouraging that our model reproduces some of the effects of thermal heterogeneity that have been found by Bloxham (2000), such as the distribution of inclination anomalies and the dispersion of inclinations at a site. Because his and our model differ in several respects, this indicates that the response to heterogeneous thermal forcing does not depend crucially on the particular assumptions of the dynamo model.

Because of the partly random character of secular variation, a sufficiently long averaging time is required to reveal significant deviations from the geocentric axial dipole in the time average magnetic field. From the change in Gauss coefficients with averaging window, we conclude that averaging over the archeomagnetic window (2000–3000 years) is barely enough to reveal the long-term paleomagnetic field structure (Carlut et al., 1999).

Our model results suggest that non-zonal structure in the time average field is persistent when the window exceeds about ten thousand years. However, this may still be too short for the Earth. On the paleomagnetic time scale, secular variation (the noise) has a larger amplitude in the geomagnetic field than it has in our model. Furthermore, when we average the model field, the Gauss coefficients are precisely known. Applied to the Earth's paleofield this would be equivalent to a global distribution of perfect data. This is of course unattainable and geographical bias and data errors complicate the task to retrieve the mean paleofield.

In addition to the latitudinal dependence of the VGP scatter, we also find a variation with longitude, attributed to the non-zonal structure of the CMB heat flow. The amplitude of secular variation correlates with boundary heat flow variations. Physically, where the convection is more vigorous (beneath regions of

high boundary heat flow), the secular variation is stronger. The minimum VGP scatter in our model is in the central Pacific, just where secular variation is weak in the historical field (and possibly also weak in the paleofield). Accordingly, variations in CMB heat flow perhaps offer an explanation for the alleged Pacific dipole window. But we also note that the longitudinal differences in the VGP dispersion are rather small in our model, on the order of one degree. It would be difficult to identify such small differences in the paleomagnetic data.

Westward magnetic drift is strongest in the Atlantic and absent in the east Pacific in our model, in qualitative agreement with the westward drift of the historical geomagnetic field. The average magnetic drift rates in our model are higher than the time-average azimuthal flow, indicating that westward drift is not wholly due to advection of frozen flux. However, the most dramatic examples of magnetic drift, the westward motion of equatorial flux spots, appear to be largely due to transport by equatorial jets. We suggest that the equatorial jets result from a thermal wind vorticity balance in the region between intense azimuthal flux tubes below the CMB. Expulsion of the tubes by fluid upwellings creates pairs of flux spots, which are carried westward by the jets.

Acknowledgements

Reviews by David Gubbins and an anonymous referee helped to improve the paper. U.R.C. thanks the Deutsche Forschungsgemeinschaft for support through grant Ch77/11. P.O. thanks the Geophysics Program of NSF for support through grant EAR0105238.

References

Bloxham, J., 1986. The expulsion of magnetic flux from the Earth's core. Geophys. J. R. Astr. Soc. 87, 669–678.

Bloxham, J., 2000. The effect of thermal core-mantle interactions on the paleomagnetic secular variation. Philos. Trans. R. Soc. London A358, 1171–1179.

Bloxham, J., Gubbins, D., 1985. The secular variation of Earth's magnetic field. Nature 317, 777–781.

Bloxham, J., Gubbins, D., 1987. Thermal core-mantle interaction. Nature 325, 511–513.

Bloxham, J., Gubbins, D., Jackson, A., 1989. Geomagnetic secular variation. Philos. Trans. R. Soc. London A329, 415–502.

Bullard, E.C., Freedman, C., Gellman, H., Nixon, J., 1950. The westward drift of the Earth's magnetic field. Philos. Trans. R. Soc. London A243, 67–92.

Carlut, J., Courtillot, V., Hulot, G., 1999. Over how much time should the geomagnetic field be averaged to obtain the mean-paleomagnetic field? Terra Nova 11, 239–243.

Christensen, U.R., Olson, P., Glatzmaier, G.A., 1998. A dynamo model interpretation of geomagnetic field structures. Geophys. Res. Lett. 25, 1565–1568.

Christensen, U.R., Olson, P., Glatzmaier, G.A., 1999. Numerical modelling of the geodynamo: a systematic parameter study. Geophys. J. Int. 138, 393–409.

Constable, C., Johnston, C., 1999. Anisotropic paleosecular variation models: implications for geomagnetic field observables. Phys. Earth Planet. Inter. 115, 35–51.

Constable, C., Johnston, C., Lund, S.P., 2000. Global geomagnetic field models for the past 3000 years: transient or permanent flux lobes? Philos. Trans. R. Soc. London A358, 991–1008.

Cox, A., 1970. Latitude dependence of the angular dispersion of the geomagnetic field. Geophys. J. R. Astr. Soc. 20, 253–269.

Doell, R.R., Cox, A.V., 1972. The Pacific geomagnetic secular variation anomaly and the question of lateral uniformity in the lower mantle. In: Robertson, E.C. (Ed.), The Nature of the Solid Earth. McGraw-Hill, New York, pp. 245–284.

Glatzmaier, G.A., Coe, R.S., Hongre, L., Roberts, P.H., 1999. The role of the Earth's mantle in controlling the frequency of geomagnetic reversals. Nature 401, 885–890.

Herrero-Bervera, E., Valet, J.-P., 2002. Paleomagnetic secular variation of the Honolulu volcanic series 33–700 ka O'ahu Hawaii. Phys. Earth Planet. Inter. 133, 83–97.

Hongre, L., Hulot, G., Khokhlov, A., 1998. An analysis of the geomagnetic field over the past 2000 years. Phys. Earth Planet. Inter. 106, 311–335.

Hulot, G., LeMouël, J.L., 1994. A statistical approach to the Earth's main magnetic field. Phys. Earth Planet. Inter. 82, 167–183.

Hulot, G., Eymin, C., Langlais, B., Mandea, M., Olsen, N., 2002. Small-scale structure of the geodynamo inferred from Oersted and Magsat satellite data. Nature 416, 620–623.

Johnson, C.L., Constable, C.G., 1995. The time averaged geomagnetic field as recorded by lava flows over the past 5 Myr. Geophys. J. Int. 122, 489–519.

Kono, M., Roberts, P.H., 2002. Recent geodynamo simulations and observations of the geomagnetic field, Rev. Geophys. 40 (4), 1013, 10.1029/2000RG000102.

Kono, M., Sakuraba, A., Ishida, M., 2000. Dynamo simulations and paleosecular variation models. Philos. Trans. R. Soc. London A358, 1123–1139.

Kuang, W., Bloxham, J., 1998. Numerical dynamo modeling: comparison with the Earth's magnetic field. In: Gurnis, M., et al. (Eds.), The Core-Mantle Boundary Region, Geodynamics Series 28. AGU, Washington, DC, pp. 197–208.

Kutzner, C., Christensen, U.R., 2002. From stable dipolar to reversing numerical dynamos. Phys. Earth Planet. Inter. 131, 29–45.

Lowes, F.J., 1974. Spatial power spectrum of the main geomagnetic field, and extrapolation to the core. Geophys. J. R. Astr. Soc. 36, 717–730.

Masters, G., Johnson, S., Laske, G., Bolton, H., 1996. A shear-velocity model of the mantle. Philos. Trans. R. Soc. London A354, 1385–1411.

McElhinny, M.W., McFadden, P.L., Merrill, R.T., 1996. The myth of the Pacific dipole window. Earth Planet. Sci. Lett. 143, 13–22.

McWilliams, M.O., Holcomb, R.T., Champion, D.E., 1982. Geomagnetic secular variation from ^{14}C dated lava flows on Hawaii and the question of the Pacific non-dipole low. Philos. Trans. R. Soc. London A306, 211–222.

Merrill, R.T., McElhinny, M.W., McFadden, P.L., 1998. The Magnetic Field of the Earth. Academic Press, San Diego.

Olson, P., Christensen, U.R., 2002. The time-average magnetic field in numerical dynamos with nonuniform boundary heat flow. Geophys. J. Int. 151, 809–823.

Olson, P., Christensen, U.R., Glatzmaier, G.A., 1999. Numerical modeling of the geodynamo: mechanisms of field generation and equilibration. J. Geophys. Res. 104, 10383–10404.

Quidelleur, X., Courtillot, V., 1996. On low-degree spherical harmonic models of paleosecular variation. Phys. Earth Planet. Inter. 95, 55–77.

Quidelleur, X., Valet, J.-P., Courtillot, V., Hulot, G., 1994. Long-term geometry of the geomagnetic field for the last five million years: an updated data base. Geophys. Res. Lett. 21, 1639–1642.

Runcorn, S.K., 1992. Polar path in geomagnetic reversals. Nature 356, 654.

Sakuraba, A., Kono, M., 1999. Effect of the inner core on the numerical simulation of the magnetohydrodynamic dynamo. Phys. Earth Planet. Int. 111, 105–121.

Secco, R.A., Schloessin, H.H., 1989. The electrical resistivity of solid and liquid Fe at pressures up to 7 GPa. J. Geophys. Res. 94, 5887–5894.

Yukutake, T., Tachinaka, H., 1969. Separation of the Earth's magnetic field into the drifting and standing parts. Bull. Earthquake Res. Inst. Univ. Tokyo 47, 65–97.

Zatman, S., Bloxham, J., 1997. Torsional oscillations and the magnetic field inside the Earth's core. Nature 388, 760–763.